Color bimodality: Implications for galaxy evolution

I. K. Baldry*, M. L. Balogh†, R. Bower**, K. Glazebrook* and R. C. Nichol‡

*Department of Physics & Astronomy, Johns Hopkins University, Baltimore, MD 21218, USA
†Department of Physics, University of Waterloo, N2L 3G1, Canada
**Department of Physics, University of Durham, DH1 3LE, UK
‡Institute of Cosmology and Gravitation, University of Portsmouth, PO1 2EG, UK

Abstract. We use a sample of 69726 galaxies from the SDSS to study the variation of the bimodal color-magnitude (CM) distribution with environment. Dividing the galaxy population by environment (Σ_5) and luminosity ($-23 < M_r < -17$), the $u-r$ color functions are modeled using double-Gaussian functions. This enables a deconvolution of the CM distributions into two populations: red and blue sequences. The changes with increasing environmental density can be separated into two effects: a large increase in the fraction of galaxies in the red distribution, and a small color shift in the CM relations of each distribution. The average color shifts are 0.05 ± 0.01 and 0.11 ± 0.02 for the red and blue distributions, respectively, over a factor of 100 in projected neighbor density. The red fraction varies between about 0% and 70% for low-luminosity galaxies and between about 50% and 90% for high-luminosity galaxies. This difference is also shown by the variation of the luminosity functions with environment. We demonstrate that the effects of environment and luminosity can be unified. A combined quantity, $\Sigma_{\rm mod} = (\Sigma_5/{\rm Mpc}^{-2}) + (L_r/L_{-20.2})$, predicts the fraction of red galaxies, which may be related to the probability of transformation events. Our results are consistent with major interactions (mergers and/or harassment) causing galaxies to transform from the blue to the red distribution. We discuss this and other implications for galaxy evolution from earlier results and model the effect of slow transformations on the color functions. [1]

1. INTRODUCTION

The study of galaxy properties in cosmology is important both for understanding the formation and evolution of galaxies and for interpreting measurements of large-scale structure. For example, it is necessary to determine the clustering bias of different types of galaxies relative to dark matter in order to accurately quantify cosmological parameters.

Galaxies were first classified based on their single-color morphological properties by Hubble in the 1920's [1]. The classification followed a sequence of increasing complexity from ellipticals (E0-E7) to lenticulars (S0) to spirals (Sa-Sc) to irregulars (Irr).[2] With the advent of color measurements, morphology-color relations were established, with early types being generally redder in optical colors than late types (for a review, see ref. [2]).

While there are many relationships between properties for various types of galaxies, color and absolute magnitude are two of the most useful variables; and unlike structural and spectral properties they are less dependent on imaging resolution and aperture effects, respectively. A color-magnitude (CM) relationship for E+S0 galaxies was shown to have a shallow slope with a small intrinsic scatter [3, 4, 5]. This was related to a metallicity-luminosity correlation, with more luminous galaxies having a higher luminosity-weighted metallicity [3, 6, 7]. Spirals also follow CM relationships but with larger intrinsic scatter [8, 9, 10, 11, 12]. For spirals, the luminosity correlations can be attributed to changes in star formation history (SFH) [13], dust attenuation [14], and/or metallicity [15].

When all types are considered together, the color function of galaxies can be approximated by the sum of two Gaussian functions that is a bimodal function [16, 17]. This argues that the natural division in the galaxy population is into two distributions; at least out to $z \sim 1$ [18]. Related spectral quantities such as from Hα emission [19],

[1] Article written 2004 August 16th. Refs. updated 2004 October 25th. To appear in AIP Proc., The New Cosmology, eds. R. E. Allen et al.
[2] The adjectives "early" and "late" were used to describe the relative positions in the morphological sequence [1]. The direction from simple to complex forms was chosen from the precedent of stellar spectral types, where early types (O+B stars) generally have more simple spectral features than late types (K+M stars). Ironically, the spectra of early-type galaxies are generally dominated by late-type stellar spectra and vice versa.

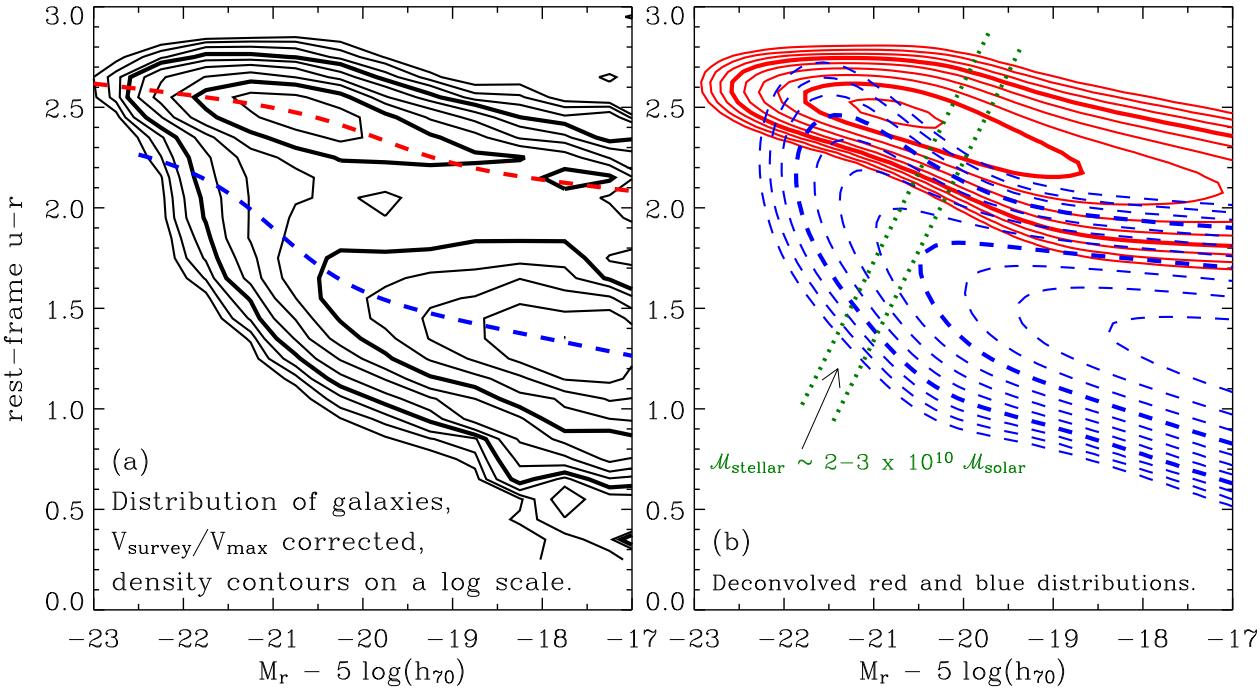

FIGURE 1. Color-magnitude distributions. (**a**): Observed bimodal distribution, corrected for incompleteness. The contours are on a logarithmic scale in number density, doubling every two levels. The dashed lines represent the color-magnitude relations of the red and blue sequences. (**b**): Deconvolved and parameterized distributions. The solid contours represent the red distribution and the dashed contours represent the blue distribution. The dotted lines represent galaxies that have similar stellar masses, near the midpoints of the transitions.

Hδ absorption and the 4000Å break [20], and the derived star formation rate (SFR) [21], also produce a bimodal distribution. In § 2, we review a quantitative study of the CM distribution of galaxies, over all environments, using a two population model; in § 3, we analyze the environmental dependence of the color bimodality; and in § 4, we discuss the results.

2. THE OVERALL COLOR-MAGNITUDE DISTRIBUTION

The Sloan Digital Sky Survey (SDSS) [22, 23, 24, 25] has dramatically improved the statistics for studying CM relations of galaxies at low redshifts: with over 10^5 redshifts and associated five color photometry for $z < 0.1$ galaxies. Baldry et al. [17] analyzed the distribution in color versus absolute magnitude of a low-redshift sample of galaxies. Figure 1(a) shows the CM distribution, corrected for incompleteness, of all galaxies (isolated, in groups and in clusters).[3] The color $u-r$ was used as it spans the 4000Å break and therefore is sensitive to star formation history. Even without a quantitative analysis, it is clear that there are two dominant sequences which can be classically associated with an E+S0 sequence (red distribution) and a spiral+irregular sequence (blue distribution).

For each magnitude bin, the color function can be approximated as the sum of two Gaussians, a bimodal function. Two possible interpretations for this are:

1. There is a continuous population but galaxies preferentially have certain colors, which depend on the luminosity. In this case, objects with intermediate colors are either transitioning or represent a middle sub-class of objects.

[3] The cosmology assumed in this article is given by $(\Omega_m, \Omega_\Lambda)_0 = (0.3, 0.7)$ with $H_0 = (h_{70})\,70\,\mathrm{km\,s^{-1}\,Mpc^{-1}}$. The data used is from the SDSS second data release [25], main galaxy sample [26], with $0.01 < z < 0.08$. This provides a sample of 69726 galaxies with 99% between r-band absolute magnitudes of -23 and -17. The magnitudes are k-corrected using a template fitting method [27].

2. There are two separate populations that have associated properties with Gaussian-like color functions (normal distributions). Here, intermediate objects are not necessarily transitioning but instead belong to one of the two populations: with a probability of being in one or the other depending on the color (and/or other properties).

In this article, we take the latter interpretation (which as shown later provides a basis for illuminating how the CM distributions vary with environment). Thus, the distribution can be deconvolved into two dominant components that have associated color-magnitude relations, dispersion-magnitude relations and luminosity functions. This is done by fitting double-Gaussian functions to the color functions separated in absolute magnitude bins. In addition, the mean and dispersion of the Gaussian are constrained to vary smoothly with magnitude.

This method differs from the classical approach of using cuts in morphology or color to define classes and instead allows for a natural overlap. The overlap could arise from: photometric errors; degeneracy between dust reddening and increasing stellar population age; stochastic variations in SFH (high past average SFR with low recent SFR can be degenerate with the opposite case); aperture effects for centrally-weighted colors[4] (bulge+disk can be degenerate with bulge only); complete degeneracy between galaxies that had different formation mechanisms.

Figure 1(b) shows the deconvolved red and blue distributions. We describe below some of the results and points to note about these sequences. For full details, see ref. [17].

1. The color-magnitude relations are not well fit by straight lines. A good fit is obtained with a straight line plus a tanh function, interpreted as a general trend plus a transition.
2. The color dispersion at the faint end of the red distribution is significantly higher than at the bright end. This is consistent with the low-luminosity red distribution galaxies forming their stars later on average that the more luminous galaxies (e.g., fig. 1 of ref. [28] shows that younger stellar populations produce a higher dispersion in CM relations). If this is the case, then the low-luminosity red sequence may not be in place at high redshift. Confirming this, recent results for clusters at $z \sim 1$ find a reduced number of galaxies in this part of the CM distribution [29, 30].
3. The blue distribution gets significantly redder for galaxies more luminous than $M_r \approx -20$. This can be interpreted as being caused by the increasing importance of dust with increasing luminosity; and a reduction in the specific SFR for the most luminous blue-distribution galaxies (which can in fact be quite red).
4. The significant overlap around $M_r \sim -21.5$ and $u-r \sim 2.4$ between the two distributions is at least partly due to a degeneracy between dust reddened late types and old stellar population early types. However, we note that the nature of the parametric fitting may overestimate the overlap.
5. If the galaxies' luminosities are converted to stellar masses, the transitions occur around the same mass as that found using spectroscopic measurements by Kauffmann et al. [20] ($3 \times 10^{10} \mathscr{M}_{\odot}$). This is an important confirmation of this transition mass using photometry, which uses apertures that scale with the size of the galaxy, as opposed to spectroscopy, which uses a $3''$ aperture (see also discussion by Kannappan [31]). The transition involves a change in the properties of both distributions and a change over in dominance from one to the other.
6. Other results suggest that galaxy environments affect the fraction of galaxies in each distribution but have little effect on the properties of galaxies within a distribution [19, 32, 33] (§ 3).

What causes the bimodality? Our results show that there must be two distinct types of galaxies: a passively evolving red population and a separate population of blue star-forming galaxies. The bimodality means that there cannot be a continuous spread in galaxy properties, and suggests that galaxies must move rapidly between the two populations. The red distribution is generally associated with (morphologically classified) early-type galaxies, which have more virialized motions of stars and less dust. Simulations have shown that major mergers can produce elliptical galaxies [34, 35, 36] and the gas or dust may be expelled by a burst of star formation [37]. Therefore, it seems reasonable that mergers (or other major interactions) are the cause of the bimodality, with the red distribution formed by violent means and the blue distribution from more quiescent accretion. In the next section, we analyze the bimodality of the CM distribution as a function of environment to test this idea further.

---

[4] Because the *u*-band has low S/N in the SDSS data, the bimodality is better quantified using 'model colors' [23] that are derived by fitting de-Vaucouleurs or exponential profiles. The profiles are defined using the *r*-band.

3. ENVIRONMENTAL DEPENDENCE

It has been known for some time that there is a higher proportion of early-type galaxies in regions of high environmental density. Dressler [38] quantified a relationship between local galaxy density and the fraction of E, S0 and spiral galaxies, with increasing E and S0 populations with increasing density. To test how the color bimodality depends on environment, we divided the galaxy population into five environmental bins.

The environmental density was estimated using a surface density given by $\Sigma_5 = 5/(\pi r^2)$ where r is the projected distance to the fifth-nearest spectroscopically-confirmed neighbor (within $\pm 1000\,\mathrm{km\,s^{-1}}$) brighter than $M_r = -20$. This is a two dimensional density given in units of Mpc^{-2}. Determining a true three dimensional density is non-trivial because of peculiar velocities. In low density regions, the conversion is approximately given by $\rho_5 = \Sigma_5/(28\,\mathrm{Mpc})$ because peculiar velocities will be small and the diameter of the cylinder ($> 8\,\mathrm{Mpc}$ for $\Sigma_5 < 0.1\,\mathrm{Mpc}^{-2}$) will be of order the height (28 Mpc at $z = 0.05$). At higher densities, for most galaxies the density will be increasingly underestimated using this conversion because galaxies will be closer together than their velocities imply. In addition, galaxies may not be observed spectroscopically because of fiber-placement restrictions and this restriction is more severe in high density regions (though we note that $> 92\%$ of the target galaxies are observed [39]). Two orders of magnitude in Σ may correspond to about three orders of magnitude in ρ (cf. fig. 4 of ref. [38]).

In cases where the edge of the survey is closer than the fifth-nearest neighbor, the distance to the boundary is used to determine an upper limit to the density while the distance to the fifth-nearest neighbor is used for a lower limit. The midpoint between the limits is used to determine which bin a galaxy falls in and galaxies are *not rejected* if (i) both limits fall in the least or most dense bin or (ii) the uncertainty in the density is less than the width of the smallest bin. From the SDSS second data release, main galaxy sample, 59085 are retained out of 69726 galaxies in the redshift range 0.01–0.08.

Figure 2 shows the $u-r$ galaxy color functions in bins of luminosity and projected density.[5] The middle density bins have equal numbers of galaxies, while the least and most dense bins have half as many. The data are fitted with double Gaussians, with the mean and amplitude of each distribution varied in all bins, while the dispersions are allowed to vary as a function of luminosity only. The data are well modeled by this parametric form. Thus, there is no major distortion to either distribution as a function of environment; and at fixed luminosity, the dominant change with environment is the fraction of galaxies in each distribution. For further discussion, see ref. [32].

Figure 3 shows the change in the fraction in the red distribution and the change in the mean color of each distribution versus environment. While the fraction on the red sequence increases by $\sim 50\%$, the mean colors only increase by 0.05 ± 0.01 and 0.11 ± 0.02 for the red and blue sequences, respectively, over a factor of 100 in projected density. Thus, we can separate two effects of increasing environmental density, major and minor: an increased trigger rate for transforming galaxies from the blue to the red distribution; and a modest reddening of each distribution, which could be caused by increasing average stellar age with increasing density. If the latter explanation were correct for the red distribution, it implies a difference in luminosity-weighted stellar age of about 1 Gyr between the lowest and highest density environments (cf. refs. [40, 41]).

The projected density has a continuous effect on the populations, at low redshift, considering both the major and minor effects. This suggests that cluster specific processes such as ram-pressure stripping [42] do not play a major role. Other work has also found that the primary effect is local density rather than cluster dynamics [32, 43, 44]. For example, Postman and Geller [43] found that the morphology-density relation was similar for galaxies in groups and in/around rich clusters.

An alternative view of the numbers in the red and blue sequences as a function of environment is given by the luminosity functions. Figure 4(a-e) shows these for the five environmental bins (with the highest density bin representing typical cluster densities). Completeness corrections were computed taking into account the magnitudes, redshifts and environmental densities of the galaxies. While the luminous cutoffs remain similar for all bins, the faint-end slopes are changing. In the highest density bin, the two sequences have a similar slope, whereas in the lowest density bin, the blue sequence has a steep slope and the red sequence a shallow slope. In particular, there are few low-luminosity red-distribution galaxies in the lowest density environmental bin, relative to blue-distribution galaxies. Note

[5] These results were determined using the SDSS second data release [25]. Earlier results presented by Balogh et al. [32] used the first data release [24]. Also, here we use Petrosian magnitudes for the absolute magnitudes, whereas the earlier results used model magnitudes. Both use model colors. The variance used for the fitting is a modified Poisson noise estimate, given by $N + 2 + (0.05\bar{N})^2$, where $\bar{N}$ is the average counts over all 28 color bins (0.45–3.25). The $+2$ term allows for a more realistic estimate of the variance for low counts; and the 5% factor allows for systematic errors and some deviation from Gaussian distributions.

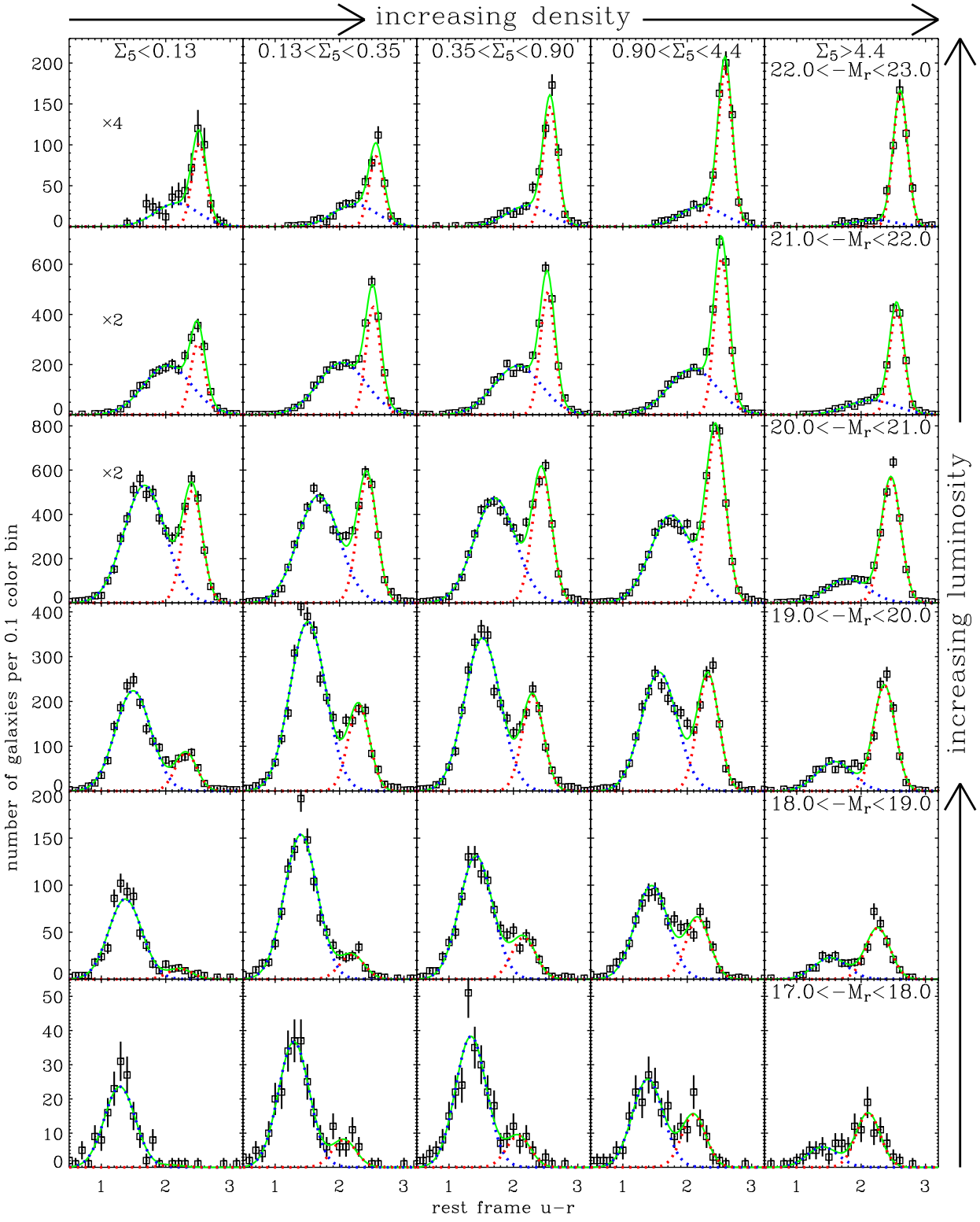

FIGURE 2. Galaxy color functions in bins of environmental density (Σ_5/Mpc^{-2}) and luminosity (M_r). The squares represent the data points with error bars, while the gray solid lines represent the double-Gaussian fits. The dotted lines represent the individual Gaussian functions. Plots where the counts have been scaled are marked $\times 2$ or $\times 4$.

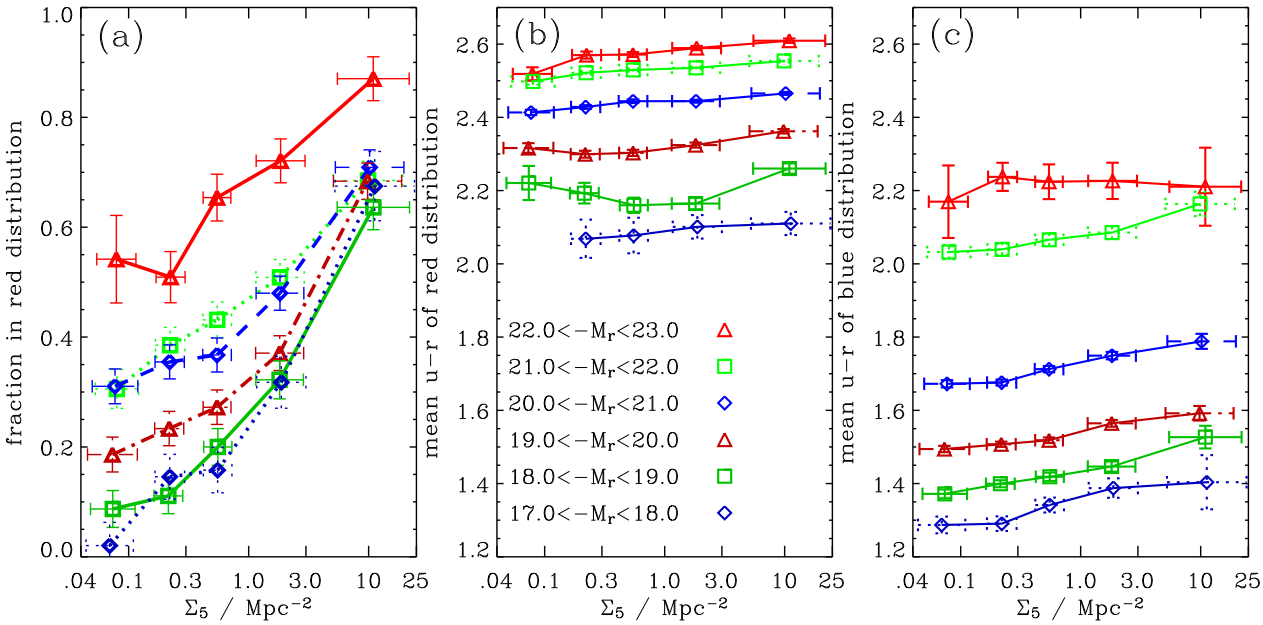

FIGURE 3. The fraction of galaxies in the red distribution (**a**) and the mean color of each distribution (**b**, **c**) as a function of environmental density. The lines and symbols represent different luminosity bins. (**b**, **c**): The average change in the mean color over a factor of 100 in Σ_5 is 0.05 ± 0.01 and 0.11 ± 0.02 for the red and blue distributions, respectively. These shifts were determined using weighted averages from straight-line fits over the six luminosity bins.

that the data are only volume limited for $M_r < -20$ and therefore the measured faint-end slopes depend significantly on large-scale structure variations with redshift (using the $V_{\rm survey}/V_{\rm max}$ method); whereas, the relative faint-end slopes do not.

It is not possible to quantitatively compare these results with previous work for two reasons: (i) this method involves a deconvolution, the double-Gaussian fitting; and (ii) the definition of red/blue (early/late) types varies slightly with density (the minor effect). Qualitatively, there is good agreement with 2dFGRS [45, 46] results, in the sense that the faint-end slopes for early- and late-type galaxies are similar in clusters [47] but different in the field [48] (see also ref. [49]). Here, the early/late division was based on a spectral type. There is disagreement with cluster LFs based on SDSS data using a cut at $u-r = 2.2$ to divide early/late [50], where the blue galaxies have a significantly steeper slope. This is because a color cut does not take account of the CM relations of the red/blue sequences (see Fig. 2, a cut at 2.2 slices the red distribution in half at low luminosities).

Figures 4(f) and 5(a-e) show the CM relations and distributions, respectively. The CM relations change slope at similar magnitudes over all the environmental densities (for the red and blue distributions, separately). In particular, the dotted lines in Fig. 5 (representing similar stellar masses) cut through the steepest part of all the CM relations. This shows that the transition mass [17, 20] is similar in all environments. Thus, this difference between low and high luminosity galaxies depends on the mass of the galaxy and not the environment. Dekel and Woo [51] suggest that this division is related to supernova feedback.

The CM distributions in Fig. 5 visually emphasize the main points of this article: (i) that the major effect with increasing density is the increase in the fraction of galaxies on the red sequence; and (ii) that, by comparison, the CM distributions of each sequence vary in a minor way, with a small shift toward redder colors with increasing density. Intriguingly, if higher-density environments went through rapid evolution but basically started from a similar population to low-density regions today, then increasing density also represents increasing time. Notably both the luminous and faint ends of the red sequence increase in number by more than the $M_r \sim -20.5$ galaxies, by transformations from the blue sequence [cf. Fig. 4(a,e)].[6] The luminous-red galaxies may have been formed by major mergers (also involving

[6] Studies looking at the mean environment [52] and clustering [53] of galaxies as a function of color and magnitude ('the other side of the coin' to our analysis), see the same effect. Here, luminous and faint red galaxies are found in more dense environments than intermediate red galaxies.

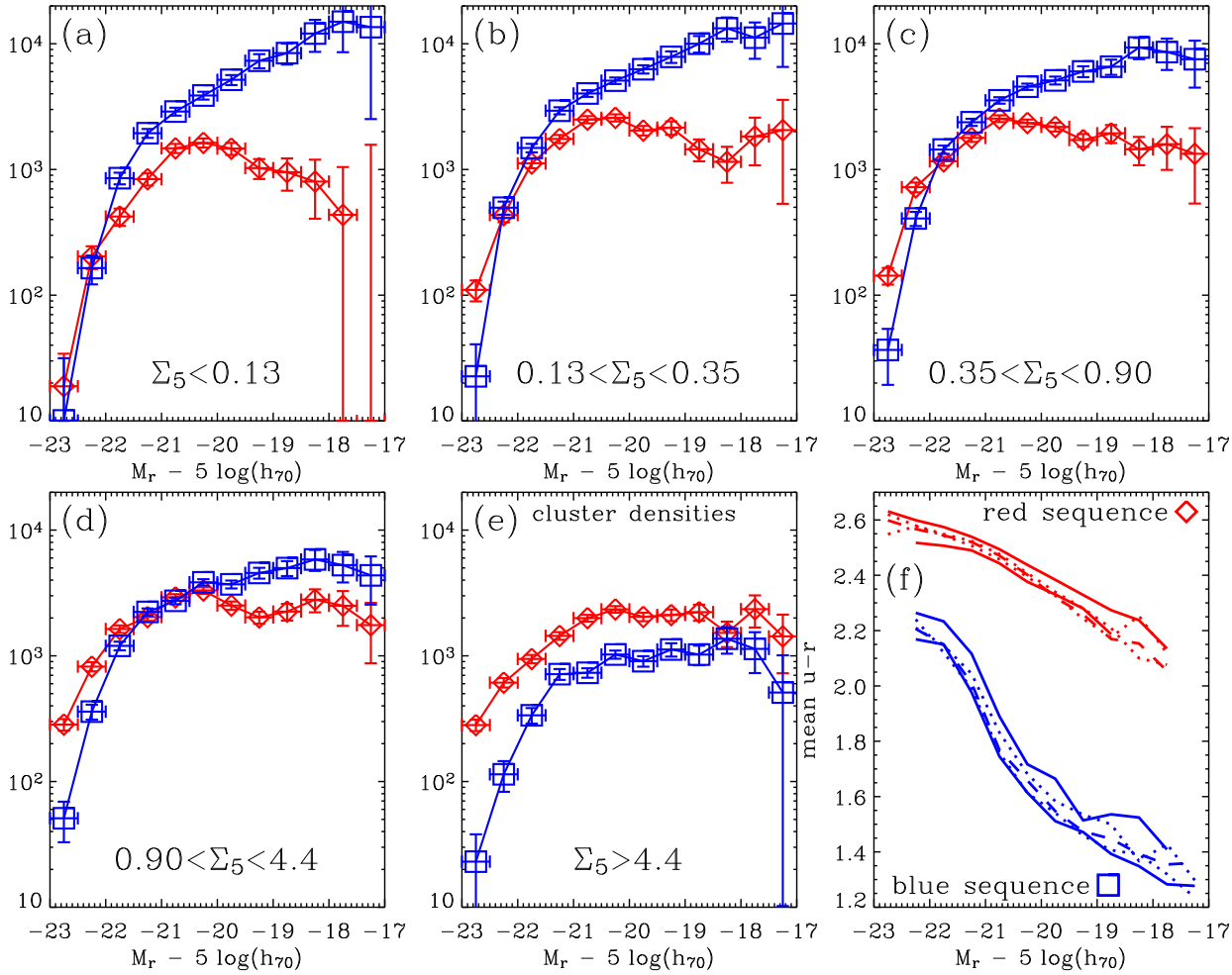

FIGURE 4. (**a**–**e**): Luminosity functions for different environmental densities. The gray squares represent the blue sequence while the diamonds represent the red sequence. The *y*-axis scale represents the completeness-corrected number per magnitude from the $0.01 < z < 0.08$ sample ($\sim 10^7$ Mpc^3). (**f**): Color-magnitude relations for all densities. The solid lines represent the lowest and highest density bins; the dashed line, the middle density bin; and the dotted lines, the remaining bins. The sequences become slightly redder with increasing density (see also Fig. 3); and they are only plotted where the error in the $u-r$ value is less than 0.07 and 0.12 for the red and blue sequences, respectively (typical formal errors are 0.01–0.04).

red-sequence galaxies) but this is unlikely to be the cause for the faint-red galaxies. This is because low-mass to low-mass galaxy mergers should be rarer than simply low-mass galaxies being 'cannibalized' by massive galaxies (minor mergers). Instead, close encounters of some kind may be enough to cause the transformation.

For our analysis, we have assumed that the color dispersions of each sequence do not depend on environment [Fig. 5(f)]. The best-fit dispersions were obtained by minimizing the combined χ^2 over all the environmental bins. Allowing the dispersions to vary would significantly increase the complexity of the double-Gaussian fitting; and the results would rely more strongly on the assumption that the distributions are exactly Gaussians. Visual inspection of Fig. 2 shows that assumption of dispersions varying with luminosity only is reasonable. There are only a couple of plots where a small change in dispersion would clearly benefit the fit (e.g. bin with $M_r = -18.5$ and $\Sigma_5 < 0.13$). This is not to say that any change in color dispersion would not be interesting (for constraining star-formation and merging histories of these galaxies [28]) but that it would require more data (future SDSS data releases) and/or a suitable technique forcing the dispersions to vary smoothly with environment and luminosity.

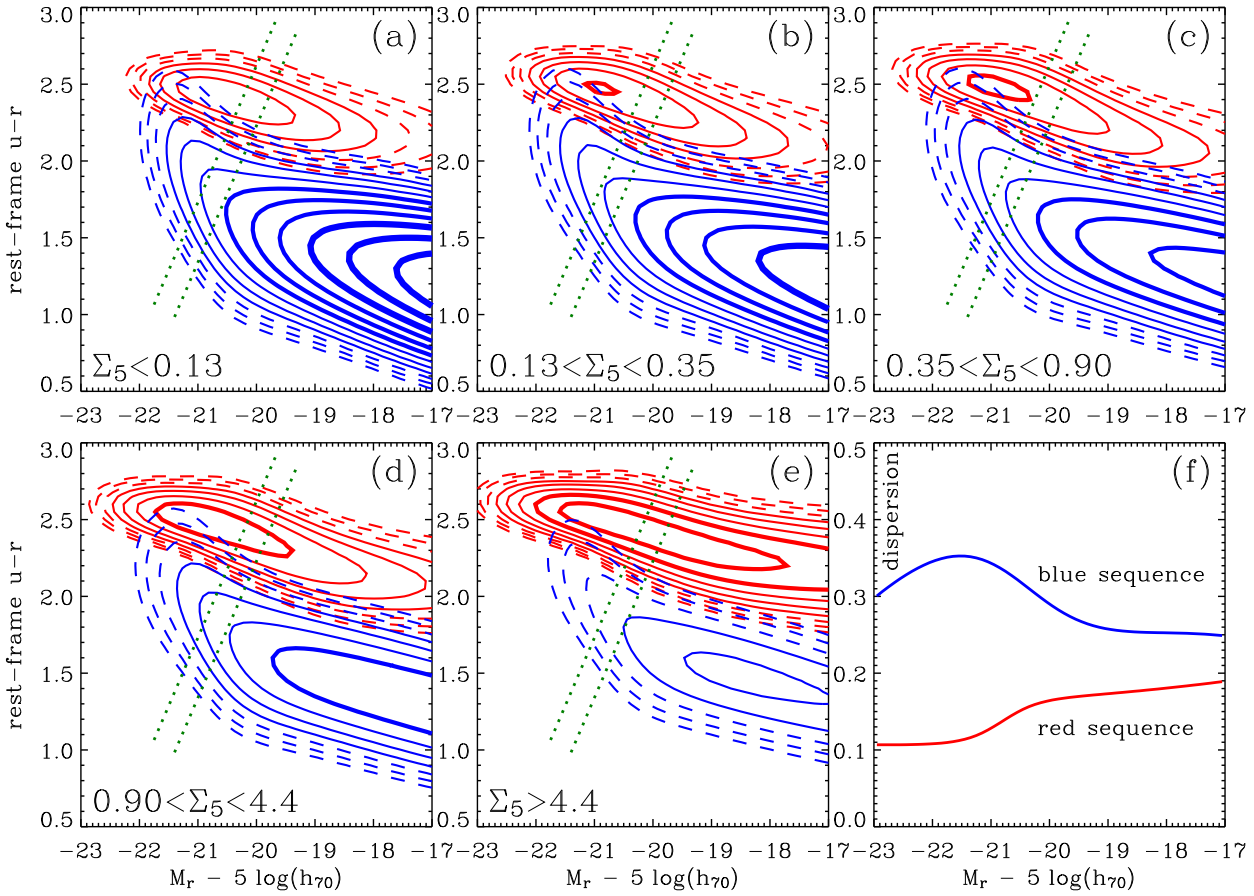

FIGURE 5. (**a**–**e**): Parameterized reconstructions of the color-magnitude distributions as a function of environmental density (normalized by total luminosity density). The gray contours represent the blue sequence while the black contours represent the red sequence. For this figure: the fitted means and dispersions have been smoothed using tanh functions plus a straight line or a quadratic; and the luminosity functions using single or double Schechter functions [17]. The dotted lines represent galaxies that have similar stellar masses (see Fig. 1). (**f**): Dispersion versus magnitude used for each sequence derived from the best fit on the *assumption* that the dispersion does not vary with density. Note that the measured dispersion includes observational uncertainties. The changes in dispersion are not obvious in Panels (a-e) because changes in the contours are generally dominated by the effects of the luminosity functions.

3.1. Combining neighbor density and luminosity

Figure 3(a) shows that there is some difference between the luminosity bins, particular at the lowest densities. There is a higher fraction of red-distribution galaxies in the most luminous bin compared to the lower luminosity bins. However, the density measure Σ_5 only measures the number density of bright neighbors and does not account for the luminosity of the galaxy in question, which could be regarded as the very local density. In other words, there must be a local density peak to form a high-mass galaxy even if that galaxy is isolated (at the present time).

To unify the luminosity and the neighbor density, we summed the two values using only one normalization parameter, which was adjusted so that the new parameter was the optimal predictor for the fraction in the red distribution. The combined quantity is given by

$$\Sigma_{\rm mod} = (\Sigma_5/{\rm Mpc}^{-2}) + (L_r/L_{-20.2})\,, \qquad (1)$$

where $L_{-20.2}$ is the fitted normalization luminosity ($5.25\times10^{21}\,{\rm W\,Hz^{-1}}$). This summation of the two terms is highly suggestive of a combined probability from an environmental and a host-galaxy mass term. Figure 6(b) shows the relationship between this modified density and the red fraction (for comparison, Fig. 6(a) uses the original density).

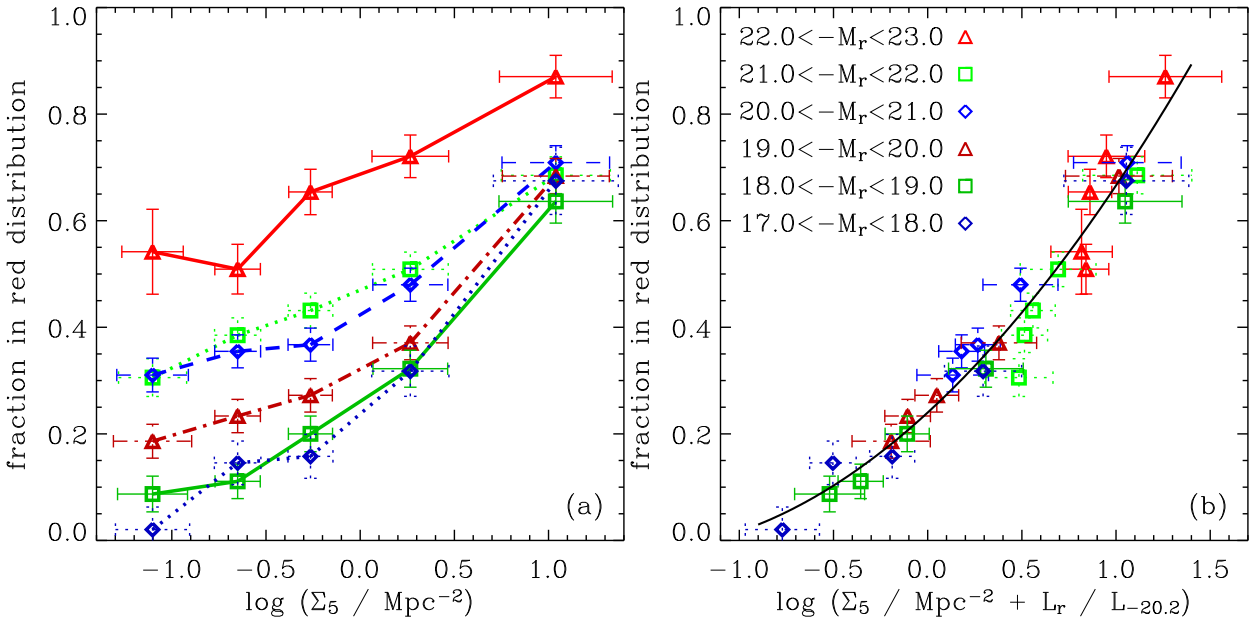

FIGURE 6. The fraction of galaxies in the red distribution as a function of environmental density. Panel (**a**) uses the projected density Σ_5 [same as Fig. 3(a)] while Panel (**b**) uses a combination of the projected density and the *r*-band luminosity (normalized by the luminosity for $M_r = -20.2$). (**b**): The solid line represents a fit to the data points using all luminosity bins.

Thus, the very local density (the mass/luminosity of the galaxy) and the neighbor density combine to produce a good predictor of whether a galaxy has been transformed to the red sequence.

This is consistent with the red distribution being formed from major interactions (mergers and/or harassment). In a hierarchical formation scenario, a present-day high-luminosity galaxy will have formed from many smaller galaxies and therefore is more likely to have undergone a violent process than a low-luminosity galaxy, regardless of environment. In other words, isolated red-distribution galaxies could be regarded as fossil groups [54, 55]. Neighbor density increases the chance of a violent process either by harassment from other galaxies [56] or by affecting the impact parameters of merging galaxies/proto-galaxies.

4. DISCUSSION

Many of the discussions in the literature have focused on quite specific mechanisms for different types of galaxies (e.g., see review by Fritze-v. Alvensleben [57] on S0 galaxies). Here, the analysis shows that there are essentially two phase spaces for galaxies (in terms of color and absolute magnitude). Even with the addition of other parameters such as surface brightness and concentration, the multi-variate distribution is bimodal [58, 59]; while bimodality is not a ubiquitous feature of semi-analytic models of galaxy formation [60, 61, 62, 63]. Perhaps the evolution of galaxies is in some sense simple. Regardless of the processes (accretion, merging, harassment, ram-pressure stripping), galaxies will populate one of two regions in parameter space and while the transformation from the blue to the red distribution may be deterministic (e.g. major merger), the properties within a distribution depend most strongly on the mass/luminosity of the galaxy and the effects of environment are mostly chaotic (e.g. the effects of minor mergers depending on impact parameters).

What about morphology? It could be argued that the CM distributions defined here are reproducing the morphology-density and CM relations of E+S0 and spiral galaxies. It is not possible to obtain Hubble types for all galaxies in the SDSS main galaxy sample because the imaging resolution is not sufficient. Nevertheless, it is unlikely that the red/blue distributions correspond precisely to these classes. Observers do not always agree on Hubble type even with many resolution elements and, in the spirit of our interpretation, whatever processes give rise to the blue/red distribution should also give rise to *distributions* in morphology. Thus, S0 or Sa galaxies could have a probability of belonging to

one or the other distributions and should not be considered as classes. The method presented in this article could be extended to include quantified morphological parameters to determine the minor/major environmental effects in terms of morphology.

What about other populations? This analysis only shows that there are two dominant populations. There are other distinct populations or distinct sub-categories. It is important to distinguish between extremes of a population and populations with separate identities. For example, passive spirals [64, 65] could be regarded as the extremes of one or both of the populations, whereas post-starburst galaxies [66, 67] could represent a separate, transforming, population. In the next section, we discuss a model that includes a significant fraction of slowly transforming galaxies.

4.1. Transformation modeling

One possibility for the trend in population abundance with environment could be that the mass function varies with local density. However, observations of the near-infrared luminosity function show that any change with environment is likely to be small [68, 69, 70]. On the other hand, the strong redshift evolution observed in the colors of galaxies in both clusters [71, 72, 73] and the field [74, 75] suggests that some galaxies transform from one population to another. In particular, Bell et al. [18] noted a build up of stellar mass on the red sequence by a factor of about two between $z \sim 1$ and 0, averaged over all environments.

Various mechanisms for these transformations have been proposed. Some, like galaxy mergers and ram-pressure stripping by the intracluster medium, occur on timescales that are short compared with the lifetime of galaxies [76, 77, 78]; other processes, such as the gradual starvation of a system through the removal of gas, result in a slow decline in star formation [79, 80].

In Fig. 7 we show the $u-r$ color evolution of two model galaxies, generated using the GALEV population-synthesis code [81]. We start with a 7 Gyr old galaxy that has been forming stars at a rate that has been slowly declining exponentially, with a timescale $\tau = 4$ Gyr. Assuming a Salpeter IMF and no dust extinction, this galaxy has a color $u-r \sim 1.4$, which is close to the peak of the observed blue distribution for the fainter galaxies in our sample.[7] In the first model, we assume all star formation activity ceases after 7 Gyr (designated $\Delta t = 0$). In this case, the galaxy rapidly becomes very red, reaching well within the observed red distribution ($u-r \sim 2$) in less than 0.2 Gyr. Therefore, if galaxies have been transforming at a uniform rate for the last 13.7 Gyr, we would only expect to see $< 1\%$ of them with intermediate colors $1.4 < u-r < 2$ (in addition to those from the two normal distributions). This would not have a noticeable effect on the simplicity of the observed bimodal population. Thus, it is possible that most or all of the red galaxies have been formed through short-timescale transformation from the star-forming blue population. This is consistent with the observed existence of galaxies with short-lived spectral features indicative of recent changes in star formation history [67, 82, 83, 84]. In this interpretation, the trend for galaxies to become slightly redder with increasing density is due to mechanisms (e.g. metallicity, dust or previous SFH) that are independent of this transformation process.

An alternative interpretation is that the transformation is more gradual, as expected in some models [79, 80] and suggested by the lack of environmental dependence of correlations between different SFH indicators [85]. The second model in Fig. 7 shows the color evolution of a galaxy in which, for $\Delta t > 0$, the SFR declines exponentially with a timescale $\tau = 2$ Gyr. This decline is still faster than that prior to $\Delta t = 0$, but is long enough that the system is observed with intermediate colors $1.4 < u-r < 2$ for a substantial amount of time (~ 3 Gyr). This could produce a significant distortion on the bimodal distribution, and might be the cause of the apparent redward shift of the mean of the blue galaxy distribution with increasing density.

To demonstrate this, we show in Fig. 8 a series of model fits to the galaxies in moderately dense environments ($0.9 < \Sigma_5 < 4.4$), where transformations from the star forming population might be expected to be most common. We restrict the fits to the population fainter than $M_r = -21$, where the blue and red populations are most distinct. The solid lines show the default, double-Gaussian model fits presented in Fig. 2. The χ^2 value for this fit, and the fraction of galaxies in the red distribution, are shown in the legend of each panel. We now assume that the mean color of the blue population is independent of density, and equal to the mean that we compute in the lowest density bin ($\Sigma_5 < 0.13$). This model is shown as the dotted line, and is a poor fit to the data with a much larger χ^2 value in all luminosity bins.

[7] The dispersion around the color peak could be for a number of reasons: (i) stochastic variations in star formation (while the general trend for a population of galaxies could be similar, the measured color could vary because of recent bursts or quiescent periods); (ii) variations in dust attenuation because of disk orientation or intrinsic levels of dust; (iii) variations in metallicity; and (iv) photometric errors.

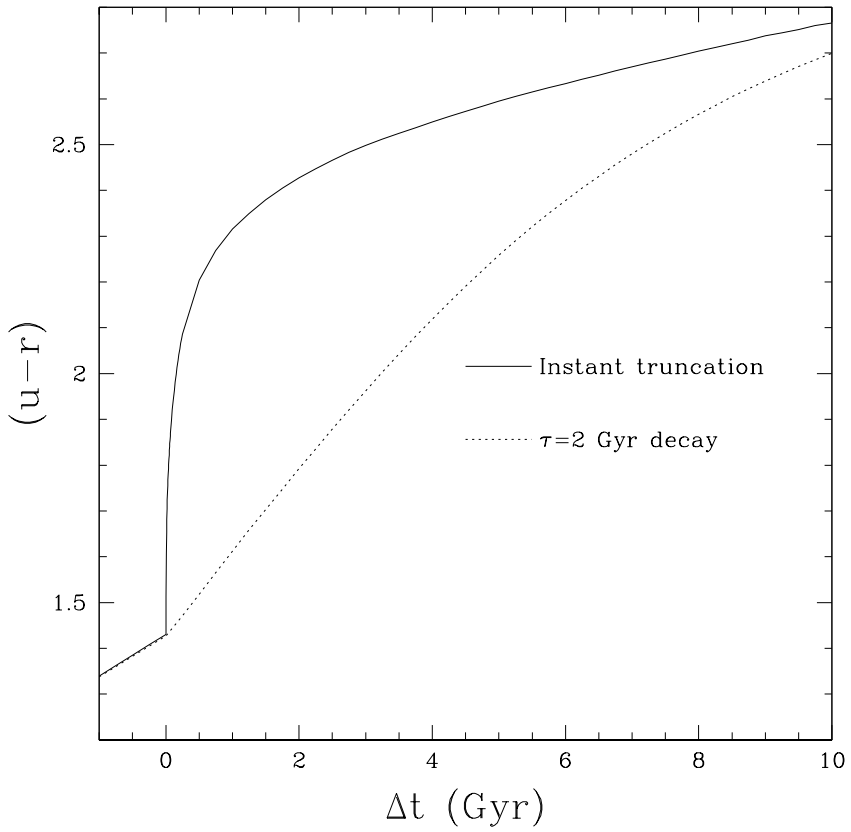

FIGURE 7. The $u-r$ color evolution of two models in which the SFR is reduced at time $\Delta t = 0$. Both models are initially evolved for 7 Gyr ($\Delta t < 0$) using a Salpeter IMF and an exponentially declining SFR with a timescale $\tau = 4$ Gyr. The *solid line* represents a model in which star formation completely ceases at $\Delta t = 0$, while the *dashed line* represents a model in which the SFR decreases exponentially with $\tau = 2$ Gyr.

To model the effect of including a transforming population, we introduce another parameter, which is the proportion of galaxies in a third population existing strictly between the means of the blue and red peaks. The color distribution of this population over this range is determined by the amount of time spent at each color, as given by the slope of the dotted line in Fig. 7. For the simple model considered here, this transforming distribution is nearly uniform in $u-r$ color. We then fit the amplitude of this population, as well as those of the red and blue Gaussian distributions, to minimize the χ^2 of the model. This fit is shown as the long-dashed line in Fig. 8. Although the χ^2 value is larger than the default two-component model, it still provides an acceptably good fit. The fraction of galaxies required to be in the transforming population is about 15%–20%; and when we account for the duty cycle of this population, up to 50% of the galaxies may have undergone such a transformation over the past 13.7 Gyr, assuming the rate has remained constant over that time.

We conclude that the best fit to the color distribution in each environment is provided by the two-population model presented in refs. [17, 32], with the possibility that the entire population of red galaxies has been built out of transformations from the bluer population that are ongoing today. These data even accommodate a relatively slow timescale for this transformation, if it is assumed that the bulk of the blue galaxy population has a mean color that is independent of environment. However, a dominance of slow transformations is likely ruled out by observations of bimodality at $z > 1.5$ [86] and by morphology-color relations, which imply a more violent origin because of bulge formation.

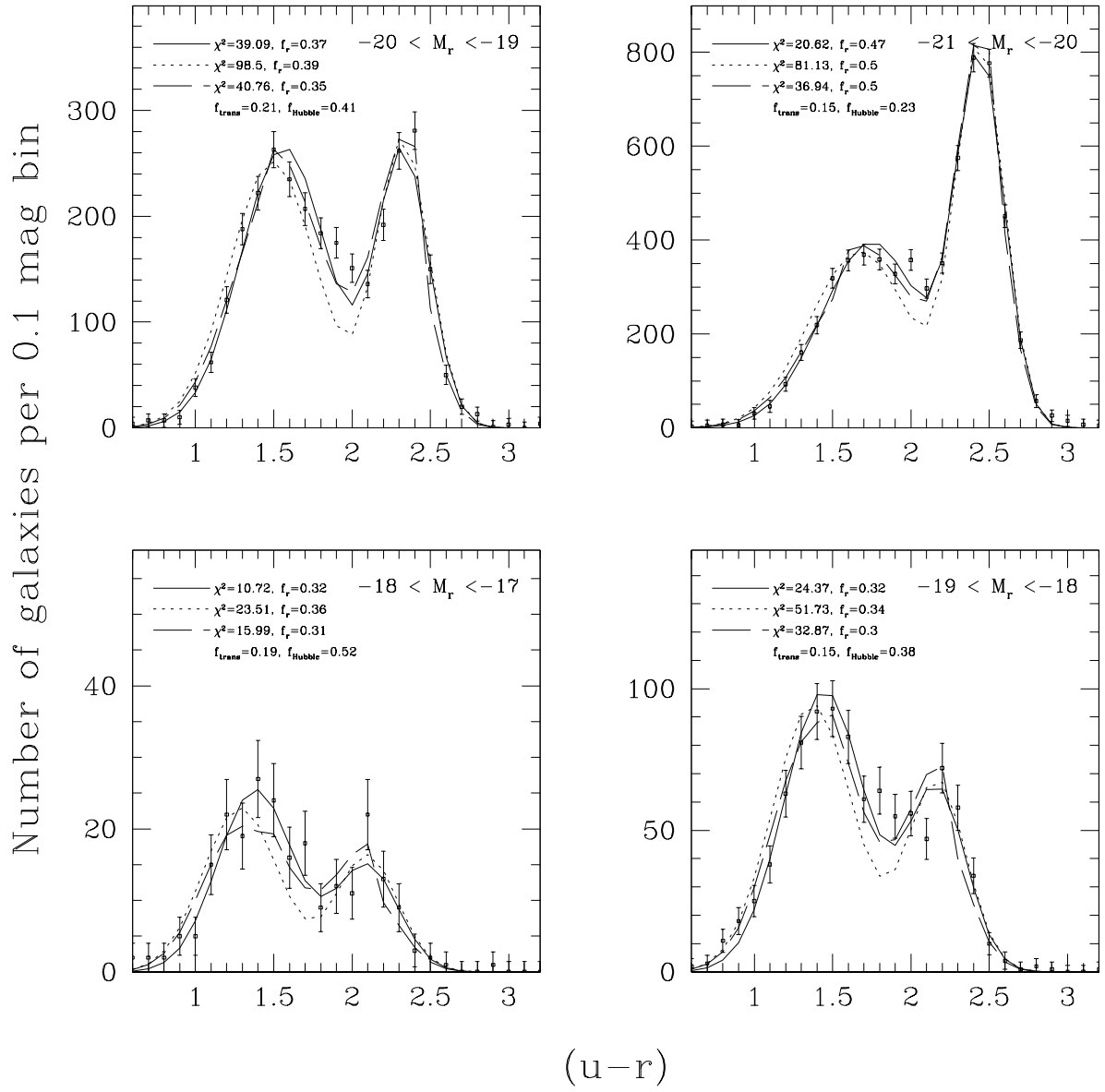

FIGURE 8. Modeling the bimodality. Observed color distributions (*points with error bars*) are shown for four luminosity bins, restricted to the second-highest density bin ($0.9 < \Sigma_5 < 4.4$). The *solid line* shows the double-Gaussian model (Fig. 2), where the mean and amplitude of each Gaussian are fit as free parameters. The *dotted line* shows the best fit obtained with the mean of the blue distribution constrained to be the same as in the fit to the lowest density bin ($\Sigma_5 < 0.13$). The *dashed line* shows the best fit obtained by adding a third component, consisting of a population of galaxies with colors intermediate between the two peaks, with a distribution given by the rate of color evolution in the $\tau = 2$ Gyr model (Fig. 7). The χ^2 values and the fraction of galaxies in the red distribution (f_r) are shown in the legend for all of these models. For the third model, the fraction of the total galaxy population comprised by these transforming galaxies at the present day ($f_{\rm trans}$) and the fraction of galaxies that would have passed through this phase in the last 13.7 Gyr ($f_{\rm hubble}$), assuming the rate of transformation has been uniform, are also shown.

ACKNOWLEDGMENTS

The results presented here made use of the CMU-PITT SDSS Value Added Catalog[8] created and maintained by K. Simon Krughoff and Christopher J. Miller. I. K. B. and K. G. acknowledge generous funding from the David and Lucille Packard Foundation. Funding for the creation and distribution of the SDSS Archive has been provided by the Alfred P. Sloan Foundation, the Participating Institutions, the National Aeronautics and Space Administration, the National Science Foundation, the U.S. Department of Energy, the Japanese Monbukagakusho, and the Max Planck Society.

REFERENCES

1. Hubble, E. P., *Astrophys. J.*, **64**, 321–369 (1926).
2. Roberts, M. S., and Haynes, M. P., *Ann. Rev. Astron. Astrophys.*, **32**, 115–152 (1994).
3. Faber, S. M., *Astrophys. J.*, **179**, 731–754 (1973).
4. Visvanathan, N., and Sandage, A., *Astrophys. J.*, **216**, 214–226 (1977).
5. Aaronson, M., Persson, S. E., and Frogel, J. A., *Astrophys. J.*, **245**, 18–24 (1981).
6. Larson, R. B., *Mon. Not. Roy. Astron. Soc.*, **169**, 229–246 (1974).
7. Kodama, T., and Arimoto, N., *Astron. Astrophys.*, **320**, 41–53 (1997).
8. Chester, C., and Roberts, M. S., *Astron. J.*, **69**, 635–640 (1964).
9. Visvanathan, N., and Griersmith, D., *Astron. Astrophys.*, **59**, 317–328 (1977).
10. Griersmith, D., *Astron. J.*, **85**, 1295–1311 (1980).
11. Visvanathan, N., *Astron. Astrophys.*, **100**, L20–L22 (1981).
12. Tully, R. B., Mould, J. R., and Aaronson, M., *Astrophys. J.*, **257**, 527–537 (1982).
13. Peletier, R. F., and de Grijs, R., *Mon. Not. Roy. Astron. Soc.*, **300**, L3–L6 (1998).
14. Tully, R. B., Pierce, M. J., Huang, J., Saunders, W., Verheijen, M. A. W., and Witchalls, P. L., *Astron. J.*, **115**, 2264–2272 (1998).
15. Zaritsky, D., Kennicutt, R. C., and Huchra, J. P., *Astrophys. J.*, **420**, 87–109 (1994).
16. Strateva, I., Ivezić, Ž., Knapp, G. R., et al., *Astron. J.*, **122**, 1861–1874 (2001).
17. Baldry, I. K., Glazebrook, K., Brinkmann, J., Ivezić, Ž., Lupton, R. H., Nichol, R. C., and Szalay, A. S., *Astrophys. J.*, **600**, 681–694 (2004).
18. Bell, E. F., Wolf, C., Meisenheimer, K., et al., *Astrophys. J.*, **608**, 752–767 (2004).
19. Balogh, M., Eke, V., Miller, C., et al., *Mon. Not. Roy. Astron. Soc.*, **348**, 1355–1372 (2004).
20. Kauffmann, G., Heckman, T. M., White, S. D. M., et al., *Mon. Not. Roy. Astron. Soc.*, **341**, 54–69 (2003).
21. Brinchmann, J., Charlot, S., White, S. D. M., Tremonti, C., Kauffmann, G., Heckman, T., and Brinkmann, J., *Mon. Not. Roy. Astron. Soc.*, **351**, 1151–1179 (2004).
22. York, D. G., et al., *Astron. J.*, **120**, 1579–1587 (2000).
23. Stoughton, C., Lupton, R. H., et al., *Astron. J.*, **123**, 485–548 (2002).
24. Abazajian, K., et al., *Astron. J.*, **126**, 2081–2086 (2003).
25. Abazajian, K., et al., *Astron. J.*, **128**, 502–512 (2004).
26. Strauss, M. A., Weinberg, D. H., Lupton, R. H., et al., *Astron. J.*, **124**, 1810–1824 (2002).
27. Blanton, M. R., et al., *Astron. J.*, **125**, 2348–2360 (2003).
28. Bower, R. G., Kodama, T., and Terlevich, A., *Mon. Not. Roy. Astron. Soc.*, **299**, 1193–1208 (1998).
29. De Lucia, G., Poggianti, B. M., et al., *Astrophys. J.*, **610**, L77–L80 (2004).
30. Kodama, T., Yamada, T., et al., *Mon. Not. Roy. Astron. Soc.*, **350**, 1005–1014 (2004).
31. Kannappan, S. J., *Astrophys. J.*, **611**, L89–L92 (2004).
32. Balogh, M. L., Baldry, I. K., Nichol, R., Miller, C., Bower, R., and Glazebrook, K., *Astrophys. J.*, **615**, L101–L104 (2004).
33. Budavári, T., Connolly, A. J., Szalay, A. S., et al., *Astrophys. J.*, **595**, 59–70 (2003).
34. Tinsley, B. M., and Larson, R. B., *Mon. Not. Roy. Astron. Soc.*, **186**, 503–517 (1979).
35. Barnes, J. E., *Astrophys. J.*, **331**, 699–717 (1988).
36. Barnes, J. E., and Hernquist, L., *Ann. Rev. Astron. Astrophys.*, **30**, 705–742 (1992).
37. Joseph, R. D., and Wright, G. S., *Mon. Not. Roy. Astron. Soc.*, **214**, 87–95 (1985).
38. Dressler, A., *Astrophys. J.*, **236**, 351–365 (1980).
39. Blanton, M. R., Lin, H., Lupton, R. H., Maley, F. M., Young, N., Zehavi, I., and Loveday, J., *Astron. J.*, **125**, 2276–2286 (2003).
40. Bernardi, M., Sheth, R. K., et al., *Astron. J.*, **125**, 1866–1881 (2003).
41. Hogg, D. W., Blanton, M. R., Brinchmann, J., et al., *Astrophys. J.*, **601**, L29–L32 (2004).

[8] `http://astrophysics.phys.cmu.edu/dr2_value_added/`

42. Farouki, R., and Shapiro, S. L., *Astrophys. J.*, **241**, 928–945 (1980).
43. Postman, M., and Geller, M. J., *Astrophys. J.*, **281**, 95–99 (1984).
44. De Propris, R., Colless, M., Peacock, J. A., et al., *Mon. Not. Roy. Astron. Soc.*, **351**, 125–132 (2004).
45. Colless, M., Dalton, G., Maddox, S., et al., *Mon. Not. Roy. Astron. Soc.*, **328**, 1039–1063 (2001).
46. Colless, M., Peterson, B. A., Jackson, C., et al., *e-Print archive* (2003), URL `arxiv.org/html/astro-ph/0306581`.
47. De Propris, R., Colless, M., Driver, S. P., et al., *Mon. Not. Roy. Astron. Soc.*, **342**, 725–737 (2003).
48. Madgwick, D. S., Lahav, O., Baldry, I. K., et al., *Mon. Not. Roy. Astron. Soc.*, **333**, 133–144 (2002).
49. Croton, D. J., Farrar, G. R., Norberg, P., et al., *Mon. Not. Roy. Astron. Soc.* (2004), submitted (astro-ph/0407537).
50. Goto, T., Okamura, S., McKay, T. A., et al., *Publ. Astron. Soc. Japan*, **54**, 515–525 (2002).
51. Dekel, A., and Woo, J., *Mon. Not. Roy. Astron. Soc.*, **344**, 1131–1144 (2003).
52. Hogg, D. W., Blanton, M. R., Eisenstein, D. J., et al., *Astrophys. J.*, **585**, L5–L9 (2003).
53. Zehavi, I., Zheng, Z., Weinberg, D. H., et al., *Astrophys. J.* (2004), submitted (astro-ph/0408569).
54. Ponman, T. J., Allan, D. J., Jones, L. R., Merrifield, M., McHardy, I. M., Lehto, H. J., and Luppino, G. A., *Nature*, **369**, 462–464 (1994).
55. Mulchaey, J. S., and Zabludoff, A. I., *Astrophys. J.*, **514**, 133–137 (1999).
56. Moore, B., Lake, G., and Katz, N., *Astrophys. J.*, **495**, 139–151 (1998).
57. Fritze-v. Alvensleben, U., "On the origin of S0 galaxies," in *Penetrating Bars through Masks of Cosmic Dust*, edited by D. L. Block et al., Springer, 2004, in press (astro-ph/0407358).
58. Hogg, D. W., Blanton, M. R., Strateva, I., et al., *Astron. J.*, **124**, 646–651 (2002).
59. Blanton, M. R., Hogg, D. W., et al., *Astrophys. J.*, **594**, 186–207 (2003).
60. White, S. D. M., and Frenk, C. S., *Astrophys. J.*, **379**, 52–79 (1991).
61. Kauffmann, G., Colberg, J. M., Diaferio, A., and White, S. D. M., *Mon. Not. Roy. Astron. Soc.*, **303**, 188–206 (1999).
62. Somerville, R. S., and Primack, J. R., *Mon. Not. Roy. Astron. Soc.*, **310**, 1087–1110 (1999).
63. Cole, S., Lacey, C. G., Baugh, C. M., and Frenk, C. S., *Mon. Not. Roy. Astron. Soc.*, **319**, 168–204 (2000).
64. Couch, W. J., Barger, A. J., Smail, I., Ellis, R. S., and Sharples, R. M., *Astrophys. J.*, **497**, 188–211 (1998).
65. Goto, T., Okamura, S., Sekiguchi, M., et al., *Publ. Astron. Soc. Japan*, **55**, 757–770 (2003).
66. Zabludoff, A. I., Zaritsky, D., Lin, H., Tucker, D., Hashimoto, Y., Shectman, S. A., Oemler, A., and Kirshner, R. P., *Astrophys. J.*, **466**, 104–113 (1996).
67. Goto, T., Nichol, R. C., Okamura, S., et al., *Publ. Astron. Soc. Japan*, **55**, 771–787 (2003).
68. De Propris, R., Eisenhardt, P. R., Stanford, S. A., and Dickinson, M., *Astrophys. J.*, **503**, L45–L48 (1998).
69. Andreon, S., and Pelló, R., *Astron. Astrophys.*, **353**, 479–486 (2000).
70. Balogh, M. L., Christlein, D., Zabludoff, A. I., and Zaritsky, D., *Astrophys. J.*, **557**, 117–125 (2001).
71. Butcher, H., and Oemler, A., *Astrophys. J.*, **285**, 426–438 (1984).
72. Fairley, B. W., Jones, L. R., Wake, D. A., Collins, C. A., Burke, D. J., Nichol, R. C., and Romer, A. K., *Mon. Not. Roy. Astron. Soc.*, **330**, 755–767 (2002).
73. Finn, R. A., Zaritsky, D., and McCarthy, D. W., *Astrophys. J.*, **604**, 141–152 (2004).
74. Lilly, S. J., Le Fevre, O., Hammer, F., and Crampton, D., *Astrophys. J.*, **460**, L1–L4 (1996).
75. Connolly, A. J., Szalay, A. S., Dickinson, M., Subbarao, M. U., and Brunner, R. J., *Astrophys. J.*, **486**, L11–L14 (1997).
76. Gunn, J. E., and Gott, J. R., *Astrophys. J.*, **176**, 1–19 (1972).
77. Fujita, Y., and Nagashima, M., *Astrophys. J.*, **516**, 619–625 (1999).
78. Moore, B., Lake, G., Quinn, T., and Stadel, J., *Mon. Not. Roy. Astron. Soc.*, **304**, 465–474 (1999).
79. Larson, R. B., Tinsley, B. M., and Caldwell, C. N., *Astrophys. J.*, **237**, 692–707 (1980).
80. Balogh, M. L., Navarro, J. F., and Morris, S. L., *Astrophys. J.*, **540**, 113–121 (2000).
81. Bruzual, G., and Charlot, S., *Mon. Not. Roy. Astron. Soc.*, **344**, 1000–1028 (2003).
82. Dressler, A., and Gunn, J. E., *Astrophys. J. Suppl.*, **78**, 1–60 (1992).
83. Poggianti, B. M., Bridges, T. J., Komiyama, Y., Yagi, M., Carter, D., Mobasher, B., Okamura, S., and Kashikawa, N., *Astrophys. J.*, **601**, 197–213 (2004).
84. Quintero, A. D., Hogg, D. W., Blanton, M. R., et al., *Astrophys. J.*, **602**, 190–199 (2004).
85. Kauffmann, G., White, S. D. M., Heckman, T. M., Ménard, B., Brinchmann, J., Charlot, S., Tremonti, C., and Brinkmann, J., *Mon. Not. Roy. Astron. Soc.*, **353**, 713–731 (2004).
86. Somerville, R. S., Moustakas, L. A., Mobasher, B., et al., *Astrophys. J.*, **600**, L135–L138 (2004).